Lower Extremity Characterization and Injury Mitigation

Brandon J. Perry, Lee Gabler, Ann Bailey, Kyvory Henderson, Fred Brozoski, Robert S. Salzar

Abstract Lower extremity injuries are among the most common seen in the event of an underbody blast (UBB) to an armored vehicle. Lower extremity accelerations typically exceed 500g with positive phase durations around 5ms while automotive rates typically peak around 250g with 10ms durations. Lack of injury criteria for UBB rates and the inability of injury criteria for automotive rates to predict lower extremity injury pose challenges for soldier safety during UBB. Until such an injury criterion exists and protective vehicle designs can be made, methods to mitigate soldier injury are essential. One potential method is to optimize the boot heel or add a protective layer on the floor of current military vehicles. To investigate effectiveness of these layers, material properties were combined with an existing lumped-mass model capable of calculating accelerations of the lower extremity. Viscoelastic materials were investigated for their ability to dissipate energy and store remaining energy long enough for the foot to disengage the floor. Sorbothane®-50 was used for two PMHS experiments to benchmark the effectiveness of injury prediction of the lumped-mass model and material mitigating properties. Inclusion of the mitigation layer reduced distal tibia accelerations by 75% for the most severe test.

Keywords Lower extremity, underbody blast, mitigation, materials

I. INTRODUCTION

The occurrence and severity of lower extremity injuries in occupants of heavily armored vehicles subject to underbody blasts (UBB) are now well known. Medical injury data from the field reveal that 32 percent of soldiers wounded in UBB events sustained foot/ankle fractures, while 16 percent sustained both foot/ankle and tibia/fibula fractures [1]. This injury mechanism is likely the result of a very stiff vehicle structure and very large improvised explosive devices [2]. This combination of structure/explosive interaction typically results in accelerations beyond 500g with positive phase durations on the order of 2 to 5ms for large, heavy vehicles [2]. This accelerative loading is greater in magnitude and much shorter in positive phase duration than those associated with automotive intrusion impacts to the lower extremities – that in the range of 100 to 250g with greater than 10ms durations [3,4]. Though automotive impact injuries are relatively well researched, there has yet to be developed an objective injury criterion for high-rate UBB events for these lower extremity injuries [5-10].

Recent advances in the understanding of the etiology of these UBB injuries and the first steps into predicting injuries from the foot-pan loading conditions have been reviewed and supplemented with data from laboratory simulations of UBB. These first steps toward the development of an injury criterion combine both relevant studies from the automotive field and recent studies focusing exclusively on the high-rate environment [11-16]. Basic biomechanical testing has been conducted to develop an automotive-rate injury criterion for axial loading of the foot/lower extremity. For example, Yoganandan et al. conducted a series of axial impact tests on the human foot/ankle complex and found a mean dynamic force at fracture (calcaneus and distal tibia) to be 15.1 kN [15]. Similarly, Funk et al. developed injury risk functions for axial loads to the foot/ankle complex from a study that included axial loads up to approximately 12 kN [16].

The appropriateness of automotive-rate tests for UBB applications can be understood by examining the different human response in each type of event. For example, in Funk et al., a test series investigating automotive intrusion produced peak toe-pan velocities of 5m/s with load durations of 10ms (an average of 50g, compared to estimates of UBB accelerations of 500+g) [16]. In that study of 43 specimens, this load rate

B. J. Perry is an MSc student, L. F. Gabler is a PhD student, A. M. Bailey is a PhD Student, K. A. Henderson is a Test Engineer, and R. S. Salzar is a Principal Scientist at the Center for Applied Biomechanics at the University of Virginia in Charlottesville, VA, USA. Fred Brozoski is a General Engineer at the US Army Aeromedical Lab in Ft Rucker, AL. (tel: 434-296-7288, fax: 434-296-3453, bjp8ce@virginia.edu).

produced 9 talus, 25 calcaneus, 7 pilon, 4 medial malleolus, 8 lateral malleolus, 2 fibula and 12 tibial plateau fractures. McKay et al. [17] observed similar injuries from higher velocity loading conditions ranging from 7.2 to 11.6 m/s with load durations of 3ms. However, the injury criterion developed by McKay et al. [17] differed from the Funk et al. [16] criterion. For the higher velocity loading, the 50 percent risk of injury from the McKay study occurred at 6.4 kN as opposed to 8.3 kN for the 50 percent injury risk reported in Funk et al. As to the question of input loading conditions encountered in UBB events, in 2001 Wang et al. reported that underbody blasts (in lighter-weight vehicles) can produce accelerations averaging 100g over timespans of 3 to 100ms [18]. Others have reported floor plate velocities produced by mine blasts to reach up to 30 m/s in 6 to 10ms [19]. With the increase in load rate, it has been demonstrated that bone increases in strength and stiffness at higher strain rates during dynamic loading [20, 21], and Schreiber et al. [22] showed a dramatic difference in bending tolerance of the human leg between quasi-static tests and dynamic tests. As the acceleration magnitude increases and the phase duration decreases, it has been observed that injuries tend to migrate from mid to lower tibia shaft to more local injuries to the calcaneus and distal tibia [7].

Until an operational injury criterion for UBB-induced lower extremity injuries can be developed and delivered to military boot and/or vehicle designers, this vulnerability will exist on vehicle platforms. In the meantime, it is important to offer guidance to vehicle designers as to methods of mitigating these injuries in currently fielded vehicles. This study combines existing biomechanical response and injury data in the lower extremity from UBB-rate loads into a lumped-mass model capable of predicting tibia loads with an optimization routine expressly for the identification of idealized injury-mitigating material properties. Further, common viscoelastic materials are characterized at high rate and used with the lumped-mass model to assess their effects on injury. In an attempt to both benchmark the accuracy of the lumped-mass model and investigate the effect of injury mitigating layers on the lower extremity, multiple tests on two separate whole body post-mortem human specimens (PMHS) were performed on the University of Virginia's UBB simulator (Figure 1) [23].

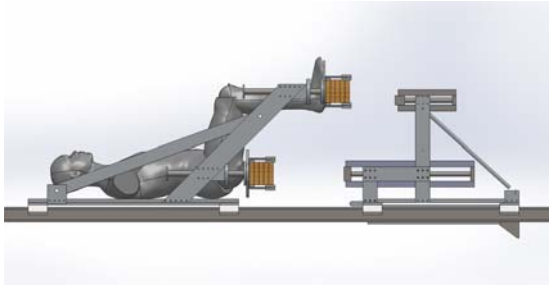

Fig. 1. Schematic of the University of Virginia UBB simulator (ODYSSEY).

II. METHODS

Two models of the lower extremity were developed for the identification and evaluation of appropriate injury mitigation materials. First, a lumped-mass model was modified from previous research and used to identify candidate materials that showed potential in reducing key accelerations in the body. Second, an existing finite element model of the lower extremity was modified for the UBB simulated environment as a more robust and accurate check on the material identification from the lumped-mass model.

Lumped-mass model of lower extremity

A modified lumped-mass model of the human lower extremity was used in this study to evaluate potential injury mitigation materials for possible inclusion in the experimental phase of this study. This model is based on the work of Henderson et al. [7] that analyzed the results from 20 drop tower tests to PMHS lower extremities. The resulting lumped-mass model and coefficients are shown in Figure 2, Table 1.

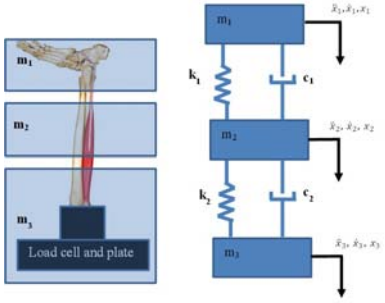

Fig. 2. Lumped-mass model of lower extremity.

Table 1
Lumped-mass model coefficients.

Coef.	Units	Mean ± 1 S.D.
k_1	kN/m	8743 ± 2263
k_2	kN/m	1198 ± 250
c_1	Ns/m	130 ± 28
c_2	Ns/m	499 ± 45
m_1	kg	1.46 ± 0.31
m_2	kg	2.66 ± 0.57
m_3	kg	9.86 ± 0.57

Finite Element model of the lower extremity

The Phase I lower extremity FE model of the GHBMC 50th percentile male, with improved heel pad properties and an increase in elements, was utilized to predict the response of a series of drop tower experiments performed by Henderson et al. [7] (Table 2). In that study, each leg was sectioned above the proximal epiphysis of the tibia and fibula, and instrumented with accelerometers, strain gauges and load cells. The legs were mounted at the bottom of a drop tower equipped with an impactor capable of producing axial loading on the PMHS foot up to 600g acceleration over 1.5ms duration. To evaluate the effect of the selected injury mitigation layer, the FE model included a preload of 100 N corresponding to the impact plate resting on top of the foot prior to impact in the experiment. A free plate attached to the potted end of the tibia via a load cell element was included in the model. Comparison between the FE model and the physical tests were made by focusing on load cell force and distal tibia strain. The finite element model used in this study was benchmarked against the results of the drop tower tests (Henderson et al.) not used for the FE formulation. The FE model demonstrates good predictability, though further refinements are expected. Each simulation case was run for 20ms using LS-DYNA V971 R6.1.1. A convergence study to ensure a proper amount of elements was performed.

Table 2
GHBMC modified mesh resolution.

Skeletal Model	Mesh Resolution (mm)
Tibia	3.8
Fibula	2.2
Calcaneus	4.7
Talus	4.1

PMHS specimens

Two (2) whole body post-mortem human subjects (PMHS) were obtained for this study for testing on the University of Virginia's Center for Applied Biomechanics UBB simulator (ODYSSEY). Both specimens were cryogenically frozen within 48 hours of death and maintained frozen until ready for use in order to ensure the biofidelity of the tissue. The target population was 50th percentile males with an upper age limit of 75 years. Both subjects were screened for infectious diseases and for pre-existing pathology that may influence the lower extremity properties. Pre-test radiographs and CT scans were taken to verify that subjects with acute or healed lower extremity fractures were excluded from this study. All DXA scores were assessed at the L3 vertebral body. All test procedures were approved by the University of Virginia institutional review board. The specimens used in this study are detailed in Table 3.

Table 3
Anthropometry of the PMHS specimens tested for benchmarking injury mitigating materials.

Subject ID	Age	Weight (kg)	Stature (cm)	DXA T-score
606	62	63.0	172.7	-0.3
622	62	82.6	180.3	-1.8

*Lunar Prodigy Advanced DXA System (GE Medical Systems LUNAR, GE Healthcare, Wauwatosa, WI, USA)

Instrumentation and positioning

Each PMHS specimen was prepared with strain gages (CEA 06-062UW-350/P2 and CEA 06-062LW-350/P2, Micro Measurements, Raleigh, NC) arranged along the long-axis of the calcaneus and tibia in the SAE-Z direction. The calcanei strain gages were placed on the medial side and the tibias were instrumented at proximal, mid and distal locations. Sufficient incisions for strain gage application were made as to allow separation between gages while disrupting minimal amounts of soft tissue. Special care was taken for strain gage application on the tibia to prevent disruption of the interosseus membrane. Bone scrapers and acetone were used to remove soft tissue from the bone. The bone was then dried using 70% isopropyl alcohol and treated with a layer of Loctite® 382™ Tak Pak® Instant Adhesive, Ultra Performance. A thin layer of Loctite was also applied to the bottom of the strain gage and pressed firmly against the treated area. Once set, strain gages were coated with air-drying acrylic (Model F006690, Micro-Measurements) to prevent moisture from interrupting the adhesive bond. Wires were glued to the bone to provide strain relief. Specimens were also fitted with accelerometers and angular rate sensors at the distal tibias and accelerometers on the proximal tibias and calcanei (see instrumentation matrix in Table 4). Accelerometer and angular rate sensors were attached to a cube and fastened to a worm-drive clamp secured tightly around the tibias. Calcanei accelerometers were attached to a fixture that was then glued to the medial side of the calcaneus. Data acquisition was performed using a combination of SLICE-PRO systems (DTS, Inc, Seal Beach, CA), and Hi-Techniques Synergy (Hi-Techniques, Inc., Madison, WI). All sensors were sampled at 1 MHz. Data were filtered to CFC1000, in accordance with SAE J211 standards [24].

Table 4
PMHS instrumentation list. All channels were sampled at 1 MHz.

Measurement	Instrument
Foot Pan and Seat Pan Accelerations SAE-Z	Endevco 7270A-20k
Left and Right Proximal and Distal Tibia Accelerations SAE-X, Z	Endevco 7264B
Left and Right Distal Tibia Angular Rates SAE-Y	DTS ARS 18k
Left and Right Calcaneus Accelerations SAE-Z	Endevco 7270A-6k
Left and Right Calcaneus and Mid and Proximal Tibia SAE-Z	CEA 06-062UW-350/P2
Left and Right Distal Tibia Strains SAE-Z	CEA 06-062LW-350/P2

Positioning of specimens was performed using 90-90-90 (degree) knee-thigh-hip angles. Specimens were each subjected to three loading conditions while simultaneously loading both the seat pan and foot pan to obtain accurate whole body kinematics. PMHS were loaded with the right foot resting on a 5 cm thick sheet of mitigating material while the left was unprotected (Table 5). The 5cm thick injury mitigation layer was selected as an upper bound in order to provide the maximum protection in the minimal amount of space inside the vehicles. Though a thicker pad could conceivably offer better protection, the limited space constraints inside a vehicle may make thicker pads impractical.

Table 5

Test matrix for benchmarking. Specimen 606 was subjected to tests 1-3 while specimen 622 was subjected to tests 4-6 (TTP is time to peak).

Test	Specimen	Velocity (m/s)	Foot Hammer Mass (kg)	Max Foot Pan Acceleration/TTP (g/ms)
1	606	5.8	33.1	155.1/0.337
2		7.2	32.4	508.2/0.288
3		13.5	32.4	655.6/0.270
4	622	6.0	33.1	123.9/0.535
5		7.3	32.4	128.5/1.091
6		13.4	32.4	507.5/1.878

Injury mitigation material selection

A UBB event causes sufficient amounts of intrusion of the floor pan into the lower extremity to cause fractures ranging from the calcaneus to the proximal tibia and fibula. A layer of a prescribed injury-mitigating material could provide sufficient protection for the lower extremity from severe levels of intrusion seen in theatre. Such a material could dissipate energy and store remaining energy long enough for disengagement of the lower extremity with the floor pan. Of course, when dealing with high acceleration/short duration events as seen in typical UBB involving heavy vehicles, it is equally important to prevent spreading of the accelerative load over such a broad time domain as to turn a UBB event into an automotive intrusion event (with lower acceleration magnitudes and much longer durations). In either event, the end result is often a severely injured lower extremity, with the only difference being the location of the fractures. For this study, both available injury criteria for UBB-rate loads to the lower extremities, as well as applicable automobile intrusion-rated criteria are evaluated.

Experimental data collection of candidate materials

Materials investigated for this study included polyurethane-20, -40, -60 and -80 and Sorbothane®-50 (Sorbothane, Inc., Kent, OH). Drop tower tests were performed on the polyurethanes to determine the viscoelastic material properties. Because no long term static load was applied, only the short-term time constants could be identified from the data, though these are the most important for most blast events. The experimental setup consisted of one-inch cubed pieces of material resting on a six degree-of-freedom steering column load cell (Robert A. Denton, Rochester Hills, Michigan). Hammer response and intrusion were measured by an Endevco 7264B-2k accelerometer and a Keyence laser displacement sensor. Drop heights required to strain the materials by approximately 50% were determined experimentally (Table 6). Sorbothane®-50 material properties are available from the manufacturer, thus Sorbothane®-50 was not subjected to drop tests [25].

Table 6
Hammer drop heights and velocities at impact for each durometer of polyurethane.

Polyurethane Durometer	20	40	60	80
Drop Height (cm)	2	4	10	16
Velocity at impact (m/s)	0.44	0.68	0.89	1.08

Material characterization

Each polyurethane durometer was characterized using Quasi-linear Viscoelastic theory (QLV). The force response, *F(δ,t)*, was analyzed for each ramp using the following hereditary integral:

$$F(\delta,t) = \int_0^t G_{red}(t-t')\frac{dF^e}{d\delta}\frac{d\delta}{dt'}dt' \quad (1)$$

where G_{red} is the reduced relaxation function, F^e is the instantaneous elastic force, δ is the displacement, t is the time and t' is a dummy variable for integration. An exponential expression was used for the instantaneous elastic force:

$$F^e(\delta) = A[e^{B\delta} - 1] \quad (2)$$

where *A* and *B* are the instantaneous elastic parameters. The reduced relaxation function was expressed as a summed exponential function as follows:

$$G_{red}(t) = G_\infty + \sum_{n-1}^{4} G_n e^{-t/\tau_n} \text{ where } G_1 + G_2 + G_3 + G_4 + G_\infty = 1 \quad (3)$$

where G_∞ is the steady-state relaxation coefficient and τ_n are the time constants corresponding to each of the relaxation coefficients, G_n. In this study, five relaxation coefficients were used. The time constants, τ_n, were initially set to decade values (τ_1 = 1 ms, τ_2 = 10 ms, τ_3 = 100 ms, τ_4 = 1 s) and later set to optimum values.

The hereditary integral (Eq. (1)) was numerically integrated in terms of the instantaneous elastic parameters, *A* and *B*, and relaxation coefficients, G_n and G_∞. A generalized reduced gradient technique was used to find an optimal solution for *A, B,* G_n and G_∞, and initially the time constants τ_n (Solver from Microsoft Excel 2003 Analysis ToolPak). For each specimen, all coefficients were determined from the ramp test data and used to validate the viscoelastic parameters by predicting the response for either another ramp test or an oscillatory validation test. In an effort to simplify the model and run-time, the time constants were fixed after initial analysis.

III. RESULTS

Each of the candidate injury-mitigating materials were characterized for inclusion in the predictive lumped-mass model of the human leg. For the polyurethanes, the determined non-linear and quasi-linear viscoelastic coefficients were determined; for the Sorbothane®, the linear viscoelastic coefficients were determined (Table 7).

Table 7
Material Coefficients for each of the Four Polyurethane Materials

Material - Durometer	Model Type	Instantaneous Elastic Response Terms- A, B	Reduced Relaxation Parameters- G_i	Time Constants- τ_i (s)
Polyurethane-20	Non-linear elastic	1.245E6, 2.328	0	0
Polyurethane-40	Non-linear elastic	4.763E6, 1.490	0	0
Polyurethane-60	Quasi-linear viscoelastic	3.318E7, 2.297	G_1 = 0.870 G_∞ = 0.130	τ_1 = 2.686E-4
Polyurethane-80	Quasi-linear viscoelastic	6.166E7, 1.985	G_1 = 0.140 G_2 = 0.717 G_4 = 0.0242 G_∞ = 0.119	τ_1 = 1.001E-5 τ_2 = 4.005E-4 τ_4 = 1.634
Sorbothane®-50	Linear viscoelastic	7.407E6, 0	G_1 = 0.812 G_2 = 0.101 G_∞ = 0.087	τ_1 = 1E-3 τ_2 =1E-2

Using the lumped-mass model of the human extremity, each of the characterized candidate injury-mitigating materials were evaluated as to their protective properties. Methods of evaluation involved comparing magnitudes of acceleration at the distal and proximal tibias, as well as in the calcaneus. The input acceleration-time history for the lumped-mass model analysis is shown in Figure 3.

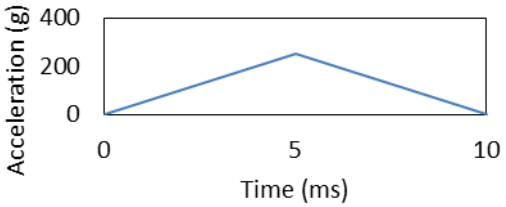

Fig. 3. Acceleration-time history for lumped-mass model analysis of candidate mitigation materials

Figure 4a shows the comparison of calcaneus accelerations for three different conditions as predicted by the lumped-mass model. First, the input pulse was applied to the model with no injury-mitigating layer. For comparison, the poorest performing injury-mitigating layer (urethane-80) is plotted, as is the best performing layer (Sorbothane®-50). Figure 4b repeats these plots at the distal tibia, where Figure 4c shows the range of acceleration mitigation for the proximal tibia. By prediction of the lumped-mass model, calcaneus accelerations could potentially be reduced by the inclusion of a 5cm thick Sorbothane®-50 layer by 56%, along with decreases in distal accelerations of 50% and in proximal accelerations by 70%.

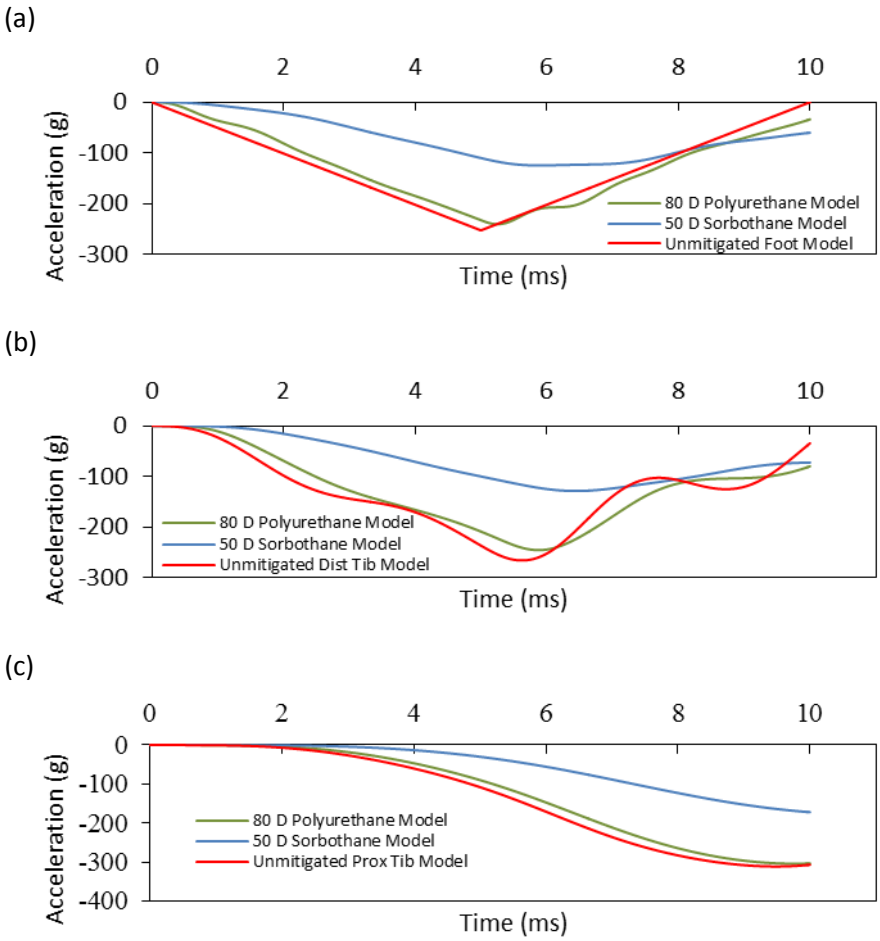

Fig. 4. (a) Comparison of calcaneus accelerations with and without injury mitigating layers; (b) Similar acceleration comparison at distal tibia; (c) Similar acceleration comparison at proximal tibia.

While the lumped-mass model was used to quickly identify the best candidate materials for the maximum possible injury mitigation, the more detailed, modified FE model of the lower extremity was used to obtain a better sense of the material's effect on the overall response. To confirm the results of the lumped-mass model, the best performing injury-mitigation material (Sorbothane®-50) was selected for the FE model validation (Figure 5) and subsequent PMHS testing (Figure 6). Each specimen was tested at subinjurious levels three times

as detailed in the test matrix shown in Table 5. Again, the left leg of each specimen had no injury mitigating layer and the right leg had the Sorbothane®-50 layer.

(a) (b)

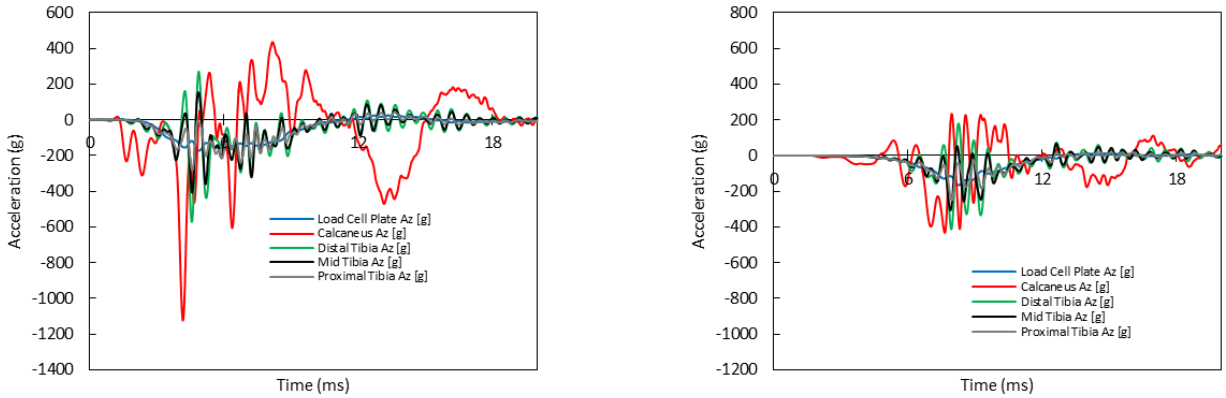

Fig. 5. Comparison of results from FE model with input shown in Figure 3: (a) Lower extremity unmitigated response; and (b) Lower extremity mitigated response using Sorbothane®-50.

(a) (d)

(b) (e)

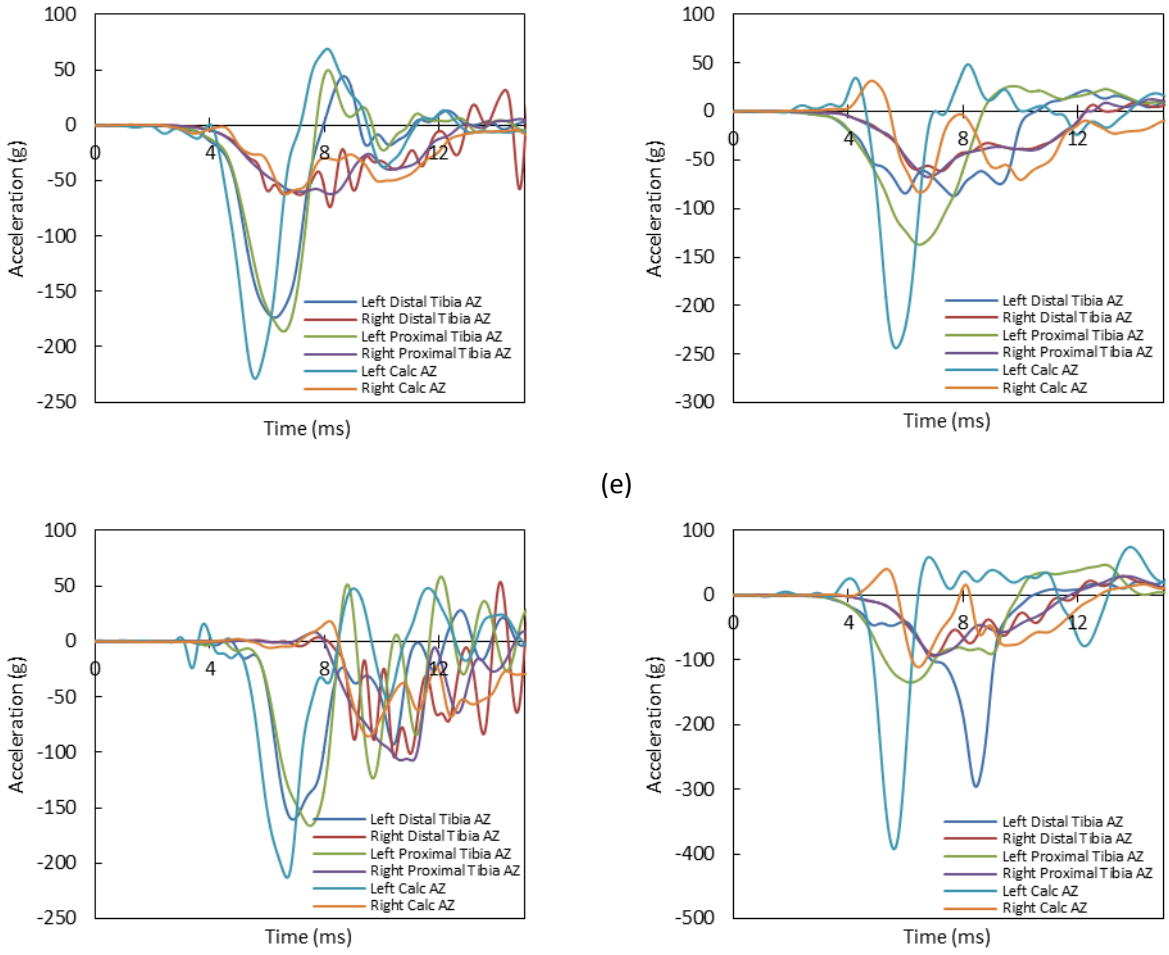

(c) (f)

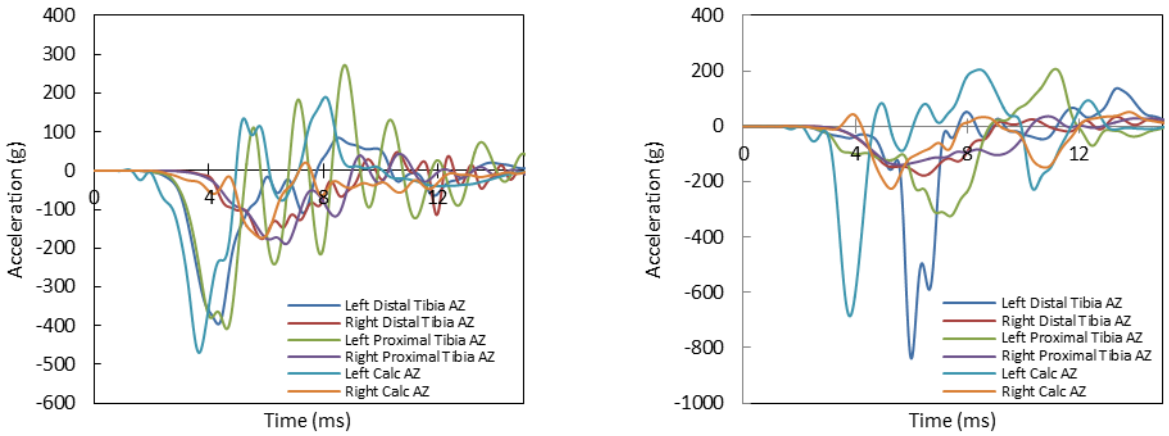

Fig. 6. (a) Experimentally measured lower extremity accelerations from Test 1; (b) Test 2; (c) Test 3; (d) Test 4; (e) Test 5; and (f) Test 6. Right leg was on injury-mitigation layer while left leg was unprotected.

In Table 8, the peak accelerations from the left lower extremities (no energy mitigating materials) are summarized along with the time to peak for the calcaneus, the distal tibia, and the proximal tibia.

Table 8
Peak lower extremity accelerations and times to peak for each test – left side, no injury mitigation material. All accelerations are in SAE-Z coordinate direction.

Test	Calcaneus		Distal Tibia		Proximal Tibia	
	Peak acceleration (g)	Time to peak (ms)	Peak acceleration (g)	Time to peak (ms)	Peak acceleration (g)	Time to peak (ms)
1	224.3	1.6	170.3	3.8	182.5	4.1
2	208.9	2.6	157.6	2.2	163.1	3.1
3	460.7	1.8	388.4	2.7	372.7	2.0
4	246.4	0.9	81.2	3.9	138.7	4.4
5	396.7	1.1	299.2	5.4	136.5	3.9
6	692.9	1.0	847.3	3.9	328.1	5.1

The peak mitigated accelerations and times to peak, and the peak unmitigated and mitigated strains and strain rates, for each test using the Sorbothane-50 are shown in Tables 9, 10, and 11, respectively.

Table 9
Peak mitigated accelerations and times to peak for each test.

Test	Calcaneus		Distal Tibia		Proximal Tibia	
	Peak acceleration (g)	Time to peak (ms)	Peak acceleration (g)	Time to peak (ms)	Peak acceleration (g)	Time to peak (ms)
1	60.9	4.4	57.0	3.2	58.7	4.6
2	84.0	1.0	102.6	1.0	105.4	2.8
3	170.3	3.8	172.8	3.2	185.6	4.4
4	84.3	1.1	61.9	4.7	68.1	4.0
5	112.4	0.6	95.1	3.9	93.7	3.5
6	227.5	1.1	179.7	4.0	140.7	5.1

Table 10
Peak unmitigated strains and strain rates.

Test	Calcaneus		Distal Tibia		Mid Tibia		Proximal Tibia	
	Peak strain (μstr)	Strain rate (μstr/ms)	Peak strain (μstr)	Strain rate (μstr/ms)	Peak strain (μstr)	Strain rate (μstr/ms)	Peak strain (μstr)	Strain rate (μstr/ms)
1	137.2	34.6	1918.5	1046.5	714.0	389.5	136.2	106.4
2	135.2	97.3	1593.3	1069.6	494.2	337.4	445.7	102.9
3	266.8	234.2	3502.1	2287.0	1624.8	496.0	574.3	111.4
4	9690.7	2852.4	2779.7	1021.4	1494.9	560.3	892.8	258.2
5	2617.5	1586.7	3617.8	1337.6	1927.6	692.1	1075.9	317.4
6	4060.8	2098.4	7624.8	792.5	4210.8	1395.8	2624.6	743.5

Table 11
Peak mitigated strains and strain rates.

Test	Calcaneus		Distal Tibia		Mid Tibia		Proximal Tibia	
	Peak strain (μstr)	Strain rate (μstr/ms)	Peak strain (μstr)	Strain rate (μstr/ms)	Peak strain (μstr)	Strain rate (μstr/ms)	Peak strain (μstr)	Strain rate (μstr/ms)
1	318.5	65.9	531.0	277.0	NA	NA	321.1	119.3
2	426.9	100.1	606.1	276.0	NA	NA	645.3	255.8
3	691.7	213.3	2019.7	872.8	NA	NA	435.8	188.5
4	183.7	96.0	1042.6	284.5	662.1	183.1	471.5	96.8
5	219.8	125.2	1096.0	331.7	641.8	181.2	361.8	92.3
6	363.8	228.3	3565.8	999.7	2327.9	636.2	1549.4	397.7

IV. DISCUSSION

Clearly, minimal amounts of injury mitigation materials can reduce calcaneus and tibia accelerations in a UBB simulated environment. Note that in most cases, the highest accelerations (in the SAE-Z direction) are located in the calcaneus (Table 8). The magnitude of accelerations seen in the tibia appears to be dependent on the magnitude of the input acceleration; that is, the higher the input acceleration, the larger the bias of peak acceleration towards the distal tibia. This can be seen most clearly in test number 6 where the distal tibia acceleration is over twice what the proximal tibia experiences. With lower input accelerations, the differences between distal and proximal tibia accelerations are smaller, indicating that the tibia is acting more as a rigid body.

Examining the right lower extremity with the injury mitigation layer, many of the same trends are seen as in the unmitigated side, but with greatly reduced magnitudes of acceleration (Table 9). Calcaneus accelerations were reduced by the mitigation layer by a range of 3 to 4 times. In Test 1, the least severe input case, calcaneus acceleration was reduced from 224g on the unmitigated side to 61g on the mitigated side. The rate-dependent trends observed in the unmitigated side also occur for the extremity with the injury mitigation layer, though the magnitudes are greatly decreased. Again, for the most severe input acceleration (Test 6), the distal acceleration is larger than that of the proximal acceleration, though this trend reverses under lesser load inputs. Comparing the times to peak between the injury mitigation side and the unmitigated side, the mitigation material did not increase the duration of the acceleration event as much as was anticipated, though in some cases a slight increase in time to peak was observed.

Examination of unmitigated strains along the length of the tibia again show how the tibia transitions from rigid body response at the lower, automobile-rate acceleration inputs to the higher, more UBB-representative rates (Table 10). Test 1 peak strains in the distal tibia are approximately 14 times that in the proximal tibia, while Test 6 peak strains in the distal tibia are approximately 3 times that in the proximal tibia. Comparing the least and most severe input cases, the strain rates between Test 1 and Test 6 show a different pattern of behavior, with the distal tibia strain rate in Test 1 at approximately 10 times that of the strain rate in the proximal tibia and the distal strain rate in Test 6 at approximately the same as that in the proximal tibia.

The strains and strain rates experienced by the injury-mitigated side of the specimens are, as expected, lower than the unmitigated side (Table 11), with peak strains in the distal tibia for Test 1 being approximately 4 times

less than that experienced on the unmitigated side, and the peak strains in the distal tibia for Test 6 being approximately half that of the unmitigated side. Strain rates were, in general, less than those seen on the unmitigated side, though the pattern is less obvious.

It is important to understand that higher, blast-rate accelerative loadings to the lower extremities will produce a different distribution of acceleration and strains along the tibia than what is seen in relatively slower automobile intrusion rate events. To effectively mitigate these blast-rate accelerations, it is important to reduce the peak input accelerations, but with the understanding that the distribution of acceleration along the length of the tibia is not proportional to the input. That is, at high rates of input acceleration, the distal tibia may experience very high accelerations due to this bias effect from rate. Decreasing the input acceleration may reduce the distal tibia acceleration, but not the mid- to proximal tibia if the body starts to behave more as a rigid body. This redistribution of accelerations, and therefore forces, may make an injury criterion suitable for blast-rate loads inappropriate, yet still predict failure in an automobile-rate criterion. A successful injury mitigation layer for UBB would prevent blast-rate fractures as well as automobile-rate fractures as a result of the mitigation material itself.

V. CONCLUSIONS

This study outlines the steps being taken to create a working injury mitigation optimization program tailored to specific UBB loads and relevant injury criteria. The first steps outlined here involve the use of a time-efficient lumped-mass model and its utility in predicting the effects of various injury-mitigating materials. This model will be incorporated into an optimization routine whereby the objective will be to minimize the values of both blast-rate and automotive injury criteria, while varying the properties of a single, multiple or a functionally-gradient layer of a viscoelastic material. A single layer of a homogeneous viscoelastic material may be insufficient to reduce both the high-rate blast injuries as well as the relatively lower rate automotive injuries.

This research has shown that the fast-running lower extremity lumped-mass model is sufficient to predict a representative response change from the addition of an injury-mitigating layer. While the lumped-mass model provides a first-order approximation of the lower extremity response, the results from the optimization model can be further investigated using a more complex, but more accurate, finite element model of the lower extremity before testing on PMHS.

VI. ACKNOWLEDGEMENT

The authors would like to thank the U.S. Department of Defense (Contract W81XWH-11-2-0086) and the U.S. Army Medical Research and Materiel Command and the U.S. Army Aeromedical Research Laboratory for their support of this research.

VII. REFERENCES

[1] Vasquez K, Logsdon K, Shivers B, Chancey C. Medical Injury Data 10 Nov 2011. Unclassified//Public Release.

[2] Ramasamy A, Hill AM, Hepper AE, Bull AMJ, Clasper JC. Blast Mines: Physics, injury mechanisms and vehicle protection. *Journal of the Royal Army Medical Corps,* 2009, 155: 258-264.

[3] Ramasamy A, Hill AM, Rhodri P, Gibb I, Bull A, Clasper J. The modern “deck-slap” injury-calcaneal blast fractures from vehicle explosions. *Journal of Trauma-Injury Infection & Critical Care, 2011, 71(6): 1694-1698.*

[4] Funk JR, Tourret L, et al. The effect of active muscle tension on the axial injury tolerance of the lower extremity. *Proceedings of the 17th International Technical Conference on the Enhanced Safety of Vehicles (ESV),* 2001, Amsterdam, Netherlands.

[5] Bir C, Barbir A, Dosquett F, Wilhelm M, van der Horst M, Wolfe G. Validation of lower limb surrogates as injury assessment tools in floor impacts due to anti-vehicular land mines. *Military Medicine*, 2008, 173(12):1180-1184.

[6] Bass CR, Folk B, et al. (2004) Development of a test methodology to evaluate mine protective footwear. *Personal Armor Systems Symposium (PASS),* 2004, The Hague, NL.

[7] Henderson K, Bailey A, Christopher J, Brozoski F, Salzar R. Biomechanical response of the lower leg under high rate loading. *Proceedings of IRCOBI Conference*, 2013, Gothenburg Sweden.

[8] McKay B, Bir C. Lower extremity injury criteria for evaluating military vehicle occupant injury in underbelly blast events. *Stapp Car Crash Journal*, 2009, 53:229-249.
[9] Quenneville C, Fraser G, Dunning C. Development of an apparatus to produce fractures from short-duration high-impulse loading with an application in the lower leg. *Journal of Biomechanical Engineering,* 2010, 132(1):014502.
[10] Wang J, Bird R, Swinton B, Krstic A. Protection of lower limbs against floor impact in army vehicles experiencing landmine explosion. *Journal of Battlefield Technology*, 2001, 4(3):11-5.
[11] Otte D, von Rheinbaben H, Zwiipp H. Biomechanics of injuries to the foot and ankle joint of car drivers and improvements for an optimal car floor development. *Proceedings of the Stapp Car Crash Conference,* 1992, Coronado, California.
[12] Crandall JR, Martin PG, et al. The influence of footwell intrusion on lower extremity response and injury in frontal crashes. *Annual Proceedings Association for the Advancement of Automotive Medicine*, 1995, Chicago, Illinois.
[13] Kruger H, Heuser G, Kraemer B, Schmitz A. Foot loads and footwell intrusion in an offset frontal crash, *Proceedings of the 14th International Technical Conference on Enhanced Safety of* Vehicles, 1995, Munich, Germany.
[14] Crandall J, Kuppa S, Klopp G, Hall G, Pilkey W, Hurwitz S. Injury mechanics and criteria for the human foot and ankle under axial impacts to the foot. *International Journal of Crashworthiness*, 1998, 3(2):147-162.
[15] Yoganandan N, Pintar F, Kumaresan S, Boynton M. Axial impact biomechanics of the human foot-ankle complex. *Journal of Biomechanical Engineering*, 1997, 119(4):433-437.
[16] Funk J, Crandall J, et al. The axial injury tolerance of the human foot/ankle complex and the effect of Achilles tension. *Journal of Biomechanical Engineering*, 2002, 124:750-757.
[17] McKay BJ, Bir CA. Lower extremity injury criteria for evaluating military vehicle occupant injury in underbelly blast events. *Stapp Car Crash Journal*, 2009, pp. 229-249.
[18] Wang J, Bird R, Swinton B, Kristic A. Protection of lower limbs against floor impact in army vehicles experiencing landmine explosion. *Journal of Battlefield Technology*, 2001, 4(3):8-12.
[19] Ramasamy A, Hill A, Masouros S, Gibb J, Bull A, Clasper J. Blast-related fracture patterns: A forensic biomechanical approach. *Journal of the Royal Society,* 2010, 8:689-698.
[20] Mather BS. Impact tolerance of the human leg. *Journal of Trauma*, 1968, 8(6):1084-1088.
[21] Martens M, van Audekercke R, deMeester P, Mulier J. The mechanical characteristics of the long bones of the lower extremity in torsional loading. *Journal of Biomechanics*, 1980, 13:667-676.
[22] Crandall JR, Portier L, et al. Biomechanical Response and Physical Properties of the Leg, Foot, and Ankle. *Society of Automotive Engineers,* 1996, 173-192.
[23] Bailey A, Christopher J, Henderson K, Brozoski F, Salzar R. Comparison of Hybrid-III and PMHS response to simulated underbody blast loading conditions. *Proceedings of IRCOBI Conference on the Biomechanics of Impact*, 2013, Gothenburg, Sweden.
[24] SAE International. Surface vehicle recommended practice. SAE J211 revised July 2007.
[25] Sorbothane®, Inc, Kent, Ohio, http://www.sorbothane.com/material-properties.php.